Superdeformations in Relativistic and Non-Relativistic Mean Field Theories

A. V. Afanasjev [1] [2] and P. Ring

Physik-Department der Technischen Universität München,
D-85747 Garching, Germany

Abstract

The applications of the extensions of relativistic mean field (RMF) theory to the rotating frame, such as cranked relativistic mean field (CRMF) theory and cranked relativistic Hartree-Bogoliubov (CRHB) theory, for the description of superdeformed bands in the $A \sim 60$, $140 - 150$ and 190 mass regions are overviewed and compared briefly with the results obtained in non-relativistic mean field theories.

PACS: 21.60.-n, 21.60.Cs, 27.50.+e, 27.60.+j, 27.70+q, 27.80.+w

[1]E-mail: anatoli.afanasjev@Physik.TU-Muenchen.DE

[2]Alexander von Humboldt fellow. On leave from Laboratory of Radiation Physics, Institute of Solid State Physics, University of Latvia, LV 2169, Salaspils, Miera str 31, Latvia

1   Introduction

Theoretical and experimental investigations of superdeformation at high spin have a long history. Starting from the prediction of such shapes within the macroscopic + microscopic method (frequently called as a cranked Nilsson-Strutinsky approach) in 70ties [1, 2] and subsequent experimental observation of the first superdeformed rotational (SD) band in ^{152}Dy by P. Twin and collaborators in 1986 [3], considerable understanding of the phenomenon of superdeformation at high spin has been reached. At present, the superdeformation at high spin has been observed in a number of mass regions, namely, $A \sim 60 - 70$ [4, 5], $A \sim 80, 130, 150, 190$ [6]. As illustrated in Fig. 1, the observed SD bands show very different patterns for the rotational behaviour depending on the deformation, on the strength of pairing correlations, and on the angular momentum content of specific SD configurations.

The experimental progress has been accompanied by the development of sophisticated theoretical models which use the concepts of mean field and the cranking model. While early detailed theoretical investigations of SD bands have been performed mainly within the macroscopic + microscopic method [8, 9, 10, 11], the fast increase of computational power allowed the development of non-relativistic microscopic models based on effective forces of Skyrme [12] or Gogny [13, 14] type and cranked versions of the relativistic mean field theory [15, 16, 17]. Review articles concerning the applications of these theoretical models to the SD bands can be found in Refs. [18, 19, 20].

Relativistic mean field (RMF) theory extended to the rotating frame has been applied in a systematic way to the description of SD bands, observed in the mass regions shown in Fig. 1, and in the present contribution, these applications are briefly overviewed with stress on the description of the quantities extracted from γ transitions within the bands and compared with some results obtained in non-relativistic mean field approaches.

2   Relativistic mean field theory in rotating frame

RMF theory describes the nucleus as a system of nucleons (Dirac spinors) which interact in a relativistic covariant manner through the exchange of virtual mesons [21]: the isoscalar scalar σ meson responsible for the large scalar attraction at intermediate distances, the isoscalar vector ω meson responsible for the vector repulsion at short distances and the isovector vector ρ meson which takes care for the asymmetry properties of nuclei with large neutron or proton excess. In addition, the photon field (A) accounts for the electromagnetic interaction.

RMF theory has been extended for the description of rotating nuclei (cranked relativistic mean field (CRMF) theory) by employing the concepts of the cranking model in Refs. [15, 16, 22] (see also Refs. [23, 24] for alternative derivations). In the first applications pairing correlations were neglected and one-dimensional cranking approximation was used. The CRMF equations include the Dirac equation in the Hartree-approximation for fermions

$$\left\{ \boldsymbol{\alpha}(-i\boldsymbol{\nabla} - \boldsymbol{V}(\boldsymbol{r})) \; + \; V_0(\boldsymbol{r}) \; + \; \beta(m + S(\boldsymbol{r})) - \Omega_x \hat{J}_x \right\} \psi_i \;\; = \;\; \epsilon_i \psi_i \tag{1}$$

where $V_0(\mathbf{r})$ represents a repulsive vector potential, $S(\mathbf{r})$ an attractive scalar potential, $\boldsymbol{V}(\boldsymbol{r})$ the magnetic potential and the term $\Omega_x \hat{J}_x$ the Coriolis field. The time-independent

inhomogeneous Klein-Gordon equations for the mesonic fields are given by

$$\left\{-\Delta - (\Omega_x \hat{L}_x)^2 + m_\sigma^2\right\} \sigma(\boldsymbol{r}) = -g_\sigma \left[\rho_s^p(\boldsymbol{r}) + \rho_s^n(\boldsymbol{r})\right] - g_2 \sigma^2(\boldsymbol{r}) - g_3 \sigma^3(\boldsymbol{r}),$$

$$\left\{-\Delta - (\Omega_x \hat{L}_x)^2 + m_\omega^2\right\} \omega_0(\boldsymbol{r}) = g_\omega \left[\rho_v^p(\boldsymbol{r}) + \rho_v^n(\boldsymbol{r})\right],$$

$$\left\{-\Delta - (\Omega_x(\hat{L}_x + \hat{S}_x))^2 + m_\omega^2\right\} \boldsymbol{\omega}(\boldsymbol{r}) = g_\omega \left[\boldsymbol{j}^p(\boldsymbol{r}) + \boldsymbol{j}^n(\boldsymbol{r})\right], \qquad (2)$$

with source terms involving the various nucleonic densities and currents

$$\rho_s^{n,p}(\boldsymbol{r}) = \sum_{i=1}^{N,Z} (\psi_i(\boldsymbol{r}))^\dagger \hat{\beta} \psi_i(\boldsymbol{r}), \qquad\qquad \rho_v^{n,p}(\boldsymbol{r}) = \sum_{i=1}^{N,Z} (\psi_i(\boldsymbol{r}))^\dagger \psi_i(\boldsymbol{r}),$$

$$\boldsymbol{j}^{n,p}(\boldsymbol{r}) = \sum_{i=1}^{N,Z} (\psi_i(\boldsymbol{r}))^\dagger \hat{\boldsymbol{\alpha}} \psi_i(\boldsymbol{r}), \qquad (3)$$

where the labels n and p are used for neutrons and protons, respectively. In the equations above, the sums run over the occupied positive-energy shell model states only (*no-sea approximation*) [25]. For simplicity, the equations for the ρ meson and the Coulomb fields are omitted in Eqs. (2) since they have the structure similar to the equations for the ω meson. Since the coupling constant of the electromagnetic interaction is small compared with the coupling constants of the meson fields, the Coriolis term for the Coulomb potential $A_0(\boldsymbol{r})$ and the spatial components of the vector potential $\boldsymbol{A}(\boldsymbol{r})$ are neglected in the calculations.

CRMF theory has been used extensively in the study of SD bands in which the pairing correlations are expected to play only a minor role. This approach has an advantage since the question of a self-consistent description of pairing correlations in finite nuclei starting from a relativistic Lagrangian still remains a not fully solved theoretical problem [26]. Considering, however, that the pairing is a genuine non-relativistic effect, which plays a role only in the vicinity of the Fermi surface one can consider the pairing correlations only between the baryons using the phenomenological Gogny interaction with finite range

$$V^{pp}(1,2) = \sum_{i=1,2} e^{-[(\boldsymbol{r}_1 - \boldsymbol{r}_2)/\mu_i]^2}$$
$$\times (W_i + B_i P^\sigma - H_i P^\tau - M_i P^\sigma P^\tau) \qquad (4)$$

in the particle-particle (pairing) channel. In conjuction with RMF theory such an approach to the description of pairing correlations has been applied, for example, in the study of ground state properties [27], neutron halos [28], and deformed proton emitters [29]. The development of Cranked Relativistic Hartree-Bogoliubov (CRHB) theory using this concept for the description of pairing correlations has been finished recently and first results have been presented at the present conference.

The CRHB equations for the fermions in the rotating frame are given in one-dimensional cranking approximation by

$$\begin{pmatrix} h - \Omega_x \hat{J}_x & \hat{\Delta} \\ -\hat{\Delta}^* & -h^* + \Omega_x \hat{J}_x^* \end{pmatrix} \begin{pmatrix} U_k \\ V_k \end{pmatrix} = E_k \begin{pmatrix} U_k \\ V_k \end{pmatrix} \qquad (5)$$

where $h = h_D - \lambda$ is the single-nucleon Dirac Hamiltonian minus the chemical potential λ and $\hat{\Delta}$ is the pairing potential. U_k and V_k are quasiparticle Dirac spinors and E_k denote the quasiparticle energies. The structure of time-independent inhomogeneous Klein-Gordon

equations for the mesonic fields is the same as in Eqs. (2) with the exception that the probabilities of the occupation of different orbitals are taken into account, when nucleonic densities and currents are calculated, by

$$\rho_s^i(\boldsymbol{r}) = \sum_{k>0} (V_k^i(\boldsymbol{r}))^\dagger \hat{\beta} V_k^i(\boldsymbol{r}), \qquad \rho_v^i(\boldsymbol{r}) = \sum_{k>0} (V_k^i(\boldsymbol{r}))^\dagger V_k^i(\boldsymbol{r})$$

$$\boldsymbol{j}^i(\boldsymbol{r}) = \sum_{k>0} (V_k^i(\boldsymbol{r}))^\dagger \hat{\boldsymbol{\alpha}} V_k^i(\boldsymbol{r}). \tag{6}$$

The sums over $k > 0$ run over all quasiparticle states corresponding to positive energy single-particle states (*no-sea approximation*) and the indexis i could be either n (neutrons) or p (protons). An additional feature is that in CRHB theory we go beyond the mean field and perform an approximate particle number projection before the variation by means of the Lipkin-Nogami method [30, 31, 32]. It turns out that this feature is extremely important for a proper description of the moments of inertia.

The spatial components of the vector mesons give origin to a magnetic potential $\boldsymbol{V}(\boldsymbol{r})$ which breaks time-reversal symmetry and removes the degeneracy between nucleonic states related via this symmetry [22, 33]. This effect is commonly referred as *nuclear magnetism* [15]. It is very important for a proper description of the moments of inertia [22]. Consequently, the spatial components of the vector ω and ρ mesons are properly taken into account in a fully self-consistent way in the calculations.

The microscopic relativistic and non-relativistic mean field approaches being fully self-consistent share some common features, for example, such as the low effective mass being typically in the range of $0.6 - 0.7$ and the presence of time-odd mean fields which have a large impact on the moments of inertia. The low values of the effective mass in microscopic theories leads to a low level density in the vicinity of the Fermi level compared with experiment. This problem can, in general, be cured by taking into account the coupling between single-particle motion and low-lying collective vibrations, see Ref. [34]. The time-odd mean fields, which play an important role in rotating nuclei, are defined uniquely in the RMF theory, while in the approaches based on effective interaction of Skyrme type this depends on underlying energy functional or the corresponding effective two-body interaction [35]. A clear advantage of RMF theory is the fact that the spin-orbit term emerges in a natural way [36], while it has to be parametrized in the non-relativistic approaches [37]. RMF theory is distinct from non-relativistic theories in the mechanism of nuclear saturation [36], where the nucleonic potential emerges as a difference of large attractive scalar ($S(\mathbf{r})$) and repulsive vector ($V_0(\mathbf{r})$) potentials.

Theoretical approaches, based on the non-relativistic macroscopic + microscopic method, which use the Woods-Saxon [9, 11, 39] or Nilsson [38] potentials for the microscopic part still remain very powerful tools for our understanding of rotating nuclei. By treating the bulk and the single-particle properties separately they have the advantage to fit many details of the actual nuclei directly to the appropriate region under investigation. However, this separation leaves some room for inconsistencies between the macroscopic and microscopic parts as illustrated, for example, in Refs. [40, 41]. In addition, time-odd mean fields are neglected in this method. However, these phenomenological models have some advantages related to the facts that (i) the effective mass is one by definition, (ii) they are more flexible due to the separation of bulk and single-particle properties, (iii) the numerical calculations are by orders of magnitude less time consuming than the ones in the microscopic approaches (see, for example, the discussion in Ref. [42]).

3 Superdeformation in the regime of weak pairing correlations.

CRMF theory has been extensively used for the description of SD bands in which the pairing correlations are expected to be considerably quenched. Detailed investigations have been performed using this approach in the $A \sim 140 - 150$ and in the $A \sim 60$ mass regions. One should clearly recognize that the neglect of pairing correlations is an approximation because pairing correlations being weak are still present even at the highest rotational frequencies. However, the question of the description of pairing correlations in the regime of weak pairing still remains an open problem (see, for example, the introduction in Ref. [33]). Almost all cranked mean field approaches which aim to describe pairing correlations in rotating nuclei use an approximate particle number projection before variation by means of the Lipkin-Nogami method, see for example Ref. [43]. However, the applicability of this method in the regime of weak pairing correlations as an approximation to exact particle number projection seems questionable [44, 45, 46]. Keeping this in mind we think that the neglect of pairing correlations is a reasonable approximation in a specific physical situations and, although some specific features such as, for example, paired band crossings cannot be addressed, it allows to gain considerable understanding of physical phenomena in the high spin region.

3.1 The $A \sim 140 - 150$ mass region

Since the discovery of superdeformation in ^{152}Dy in 1986 [3], this mass region was the testing field for different theoretical models and concepts. Already the investigations within the macroscopic + microscopic method gave an understanding of the impact of different single-particle orbitals on the dynamic moments of inertia $J^{(2)}$ and transition quadrupole moments Q_t [8, 9], possible underlying mechanisms of identical bands (see Ref. [19] and references therein), methods of configuration assignment based on properties of dynamic moments of inertia [8] or effective alignments i_{eff} [47, 48] (or similar methods), considerable quenching of pairing correlations [9, 50] and so on. These developments are covered in review articles [18, 19].

A systematic investigation of the properties of the SD bands in this mass region has been performed in the framework of the CRMF theory in Refs. [33, 7, 51, 52, 53, 54]. Using mainly the NL1 parametrization of RMF Lagrangian [25], which has only 7 parameters fitted in the middle of 80ties to the properties of several spherical nuclei, it was shown that CRMF theory reproduces well the experimentally observed features such as the properties of dynamic moments of inertia $J^{(2)}$, single-particle ordering in the SD minimum, alignment properties of single-particle orbitals etc. Calculated charge quadrupole moments Q_0 are in general somewhat larger than the average experimental values quoted in literature but they are still within the experimental error bars if the uncertainties due to stopping powers ($\sim 15\%$) are taken into account. The last feature is also typical for other theoretical approaches based either on the Nilsson or the Woods-Saxon potentials [9, 48] and Skyrme forces [55] (see also the discussion in Ref. [33]).

The overview of all these results definetely goes beyond the scope of the present article, especially considering the fact that Refs. [7, 33, 51, 54] contain detailed discussions of the relation between CRMF results and the ones obtained in non-relativistic mean field approaches. In the present review we would like to point out that the CRMF theory is able

to describe reasonably well the alignment properties of the single-particle orbitals despite the fact that no information on single-particle properties has been taken into account during the fit of the parameters of the RMF theory. Fig. 2 compares the effective alignments of specific single-particle orbitals active at superdeformation in the nuclei around ^{152}Dy obtained in the CRMF theory and cranked Nilsson-Strutinsky (CNS) approach based on the Nilsson potential with experimental values. The CRMF theory reproduces in average the experimental i_{eff} values better than the CNS approach. The descripancy between CRMF calculations and experiment seen in Fig. 2a at $\Omega_x \leq 0.5$ MeV is most likely due to the fact that pairing correlations play some role at low rotational frequency in the ^{149}Gd(1) band, see Ref. [7]. One should note, however, that with exception of the $[651]3/2(r = \pm i)$ orbitals the results of the CNS calculations are also reasonably close to experimental data.

Effective (or relative) alignments are important ingredients of our understanding of the underlying mechanism of the appearance of identical and non-identical bands [19]. Indeed, the fractional change in $J^{(2)}$ of two bands A and B (the criterion most frequently used for the selection of identical bands) is proportional to the derivative $di_{eff}^{A,B}/d\Omega_x$ [19]. Since the slope of experimental and theoretical i_{eff} values as a function of Ω_x is similar in many cases (see Fig. 2), it is clear that also the difference between $J^{(2)}$ values of compared bands is reproduced reasonably well in these cases (see Ref. [7]). Systematic investigation of effective (relative) alignments in this mass region has been performed so far only in the CNS approach based on the Nilsson potential (see Refs. [47, 48, 49] and references quoted in Ref. [7]) and in the CRMF theory [7, 51, 54]. So far, only the effective alignments associated with the $\pi[301]1/2$ orbital have been studied within the cranked Hartree-Fock approach using variuos Skyrme forces [35].

Phenomenological approaches based on cranked Nilsson or Woods-Saxon potentials have been extensively used in this mass region, see Ref. [20] and references therein. Among the microscopic non-relativistic approaches only the approaches (CHF or cranked Hartree-Fock-Bogoliubov (CHFB)) based on the effective forces of the Skyrme type have been used in a systematic way in nuclei around ^{152}Dy [35, 56, 57, 58]. While in the CRMF theory, the calculated dynamic moments of inertia $J^{(2)}$ are close to experimental data (see Refs. [33, 51, 54]), the calculations based on Skyrme forces overestimate the magnitude of $J^{(2)}$ typically by 10%.

3.2 The $A \sim 60 - 70$ mass region

As illustrated in Fig. 1, the rotational properties of the SD band in ^{60}Zn are distinctly different from the ones seen in the $A \sim 150$ and 190 mass regions. Indeed, at the highest rotational frequencies the dynamic moment of inertia $J^{(2)}$ is only approximately 60% of the kinematic moment of inertia $J^{(1)}$. The comparative study of SD and highly deformed bands in this mass region has been performed within the framework of the CRMF theory and CNS approach based on the Nilsson potential in Refs. [59, 4, 5]. Defining the spin values of the unlinked SD and highly deformed bands by means of effective alignment approach [47], it was shown that also other bands of these types show the same relation between $J^{(1)}$ and $J^{(2)}$, see Fig. 3. These features are very similar to the ones seen in smooth unfavoured terminating bands observed in the $A \sim 110$ mass region [60, 61, 42] and in a similar way they have been attributed to the influence of the limited angular momentum content of the single-particle configurations of the observed bands. For example, in the case of the ^{60}Zn SD band, one obtains from the distribution of particles and holes over

high- and low-j orbitals the "maximum" spin of the $[22, 22]^+$ configuration as $I = 36^+$. As a result, this band is three transitions away from the "maximum" spin. However, the states of the "maximum" spin are calculated triaxial both in the CRMF and in the CNS approaches. Thus, contrary to the smooth terminating bands, the SD bands do not terminate in the non-collective single-particle state at "maximum" spin in the calculations. This behavior can be understood as caused by the interaction between low-j and high-j orbitals in the $N = 3$ shell at high rotational frequencies [59]. The calculations suggest that these bands can be continued beyond the "maximum" spin in a similar way as it happens in the cranked harmonic oscillator, see Ref. [42] and references therein.

The above mentioned general features of the SD bands in the $A \sim 60 - 70$ mass region are in line with a previous study [62], where it was shown that the relation between $J^{(1)}$ and $J^{(2)}$ is not so much determined by the deformation (at $I = 0$), but rather how far away the band is from its "maximum" spin value. For example, large differences between $J^{(1)}$ and $J^{(2)}$ are not expected in the SD bands in the $A \sim 150$ mass region (see middle panel in Fig. 1) because the "maximum" spin of their configurations, $I_{max} \sim (150 - 200)\hbar$, is far above the experimentally accessible spin values (see Ref. [62]). An additional consequence of the fact that SD and highly deformed bands in the mass region of interest are coming close to the "maximum" spin is a gradual drop of collectivity (i.e. a drop of the transition quadrupole moment Q_t) with increasing spin which is larger than the one expected in the $A \sim 150$ mass region, see Fig. 4 in Ref. [59] and Ref. [33].

It turns out that the rotational properties ($J^{(1)}$ and $J^{(2)})^3$, effective alignments i_{eff} and transition quadrupole moments Q_t of highly deformed and SD bands are described very well both in the CRMF and in the CNS approaches, see Refs. [59, 4, 5] and Fig. 3 in the present manuscript, with the results of CRMF calculations being in average in better agreement with experimental data.

The structure of the highly deformed and SD bands in this mass region has been studied also in other approaches. The CHF calculations with an effective forces of the Skyrme type have been performed in Refs. [63, 64, 65]. The SD band observed in ^{62}Zn has been extensively studied both in the CRMF theory and in the CHF approach with Skyrme forces in Ref. [66] using different parametrizations of the RMF Lagrangian and effective forces. The projected shell model which goes beyond mean field approximation has been used in the study of SD bands in Ref. [67].

4   Superdeformation in the $A \sim 190$ mass region.

The SD bands in this mass region are in most cases characterised by the dynamic moment of inertia $J^{(2)}$ which increases with increasing rotational frequency, see Fig. 4. Kinematic moments of inertia $J^{(1)}$ of linked SD bands in ^{192,194}Pb and ^{194}Hg (see Fig. 5) show the same features and in addition the relation $J^{(2)} \geq J^{(1)}$ holds. This indicates that the pairing correlations play a more important role in these bands compared with the ones observed in the $A \sim 60$ and 150 mass regions, see Sect. 4.

Different non-relativistic approaches have been employed for the study of the superdeformation in this mass region. The CHFB calculations of SD bands in this mass region have been performed using Gogny forces without [13] and with [68, 69, 70] approximate particle number projection before variation by means of Lipkin-Nogami method. The

---

[3]The description of the paired band crossing observed in ^{60}Zn band at $\Omega_x \sim 1.0$ MeV is not addressed in the present calculations without pairing.

calculations using Gogny forces with diagonalization of the collective Bohr Hamiltonian with the inertial functions calculated at zero spin via the Gaussian Overlap Approximation to the Generator Coordinate Method have been performed in Refs. [68, 71]. A clear advantage of the microscopic theories based on the effective forces of the Gogny type is that no additional parameters are needed to describe the pairing correlations.

On the other hand, theoretical approaches discussed below use some assumptions about the type of pairing interaction and fit its parameters to the experimental data. An extensive investigation of SD bands in this mass region has been performed within the CHFB approach with effective forces of the Skyrme type in Refs. [72, 73, 74, 75, 76]. It was concluded that special attention should be taken to the effective interaction in the pairing channel and that surface active delta pairing gives a better agreement with data for the behaviour of the dynamic moment of inertia $J^{(2)}$ versus rotational frequency than either the volume active or the seniority pairing [74]. The CHFB approach based on the Woods-Saxon potential together with Lipkin-Nogami method for approximate particle number projection has been developed in Refs. [77, 78]. This approach has been used frequently in the investigation of SD bands observed in different mass regions (see Ref. [20] and references quoted therein). It employs monopole and quadrupole pairing in the particle-particle (pairing) channel. Monopole+quadrupole pairing has also been used in the projected shell model calculations of the SD bands in this mass region [79]. Note, however, that the later approach goes beyond the mean field approximation.

Cranked Relativistic Hartree-Bogoliubov theory (see Sect. 2) has been applied to the description of the SD bands observed in even-even nuclei with neutron numbers $N = 110, 112, 114$ [17]. The calculations have been performed with the NL1 parametrization [25] of the relativistic mean field Lagrangian and the D1S set of the parameters for the Gogny force [80]. The results of the calculations for the dynamic and the kinematic moments of inertia are shown in Figs. 4, 5. One can see that a very successful description of rotational features of experimental bands is obtained in the calculations without adjustable parameters. A comparison with results of other approaches based on the mean field concept (see, for example, Fig. 3 in Ref. [77], Figs. 1 and 8 in Ref. [74], Fig. 1 in Ref. [69], Figs. 5 and 6 in Ref. [70] and Fig. 1a in Ref. [68]) and the projected shell model (see Figs. 1 and 2 in Ref. [79]) indicates that the CRHB calculations provide one of best agreements with experimental data. The calculated values of transition quadrupole moments Q_t are also close to the measured ones, however, more accurate and consistent experimental data on Q_t is needed in order to make detailed comparisons between experiment and theory, for details see the discussion in Ref. [17]. RMF theory also excellently reproduces the excitation energies of the SD bands relative to the ground state in ^{194}Hg and ^{194}Pb nuclei [81].

The increase of kinematic and dynamic moments of inertia in this mass region can be understood in the framework of CRHB theory as emerging predominantly from a combination of three effects: the gradual alignment of a pair of $j_{15/2}$ neutrons, the alignment of a pair of $i_{13/2}$ protons at a somewhat higher frequency, and decreasing pairing correlations with increasing rotational frequency. The interplay of alignments of neutron and proton pairs is more clearly seen in the Pb isotopes where the calculated $J^{(2)}$ values show either a small peak (for example, at $\Omega_x \sim 0.45$ MeV in ^{192}Pb, see Fig. 4) or a plateau (at $\Omega_x \sim 0.4$ MeV in ^{196}Pb, see Fig. 4). With increasing rotational frequency, the $J^{(2)}$ values determined by the alignment in the neutron subsystem decrease but this process is compensated by the increase of $J^{(2)}$ due to the alignment of the $i_{13/2}$ proton pair. This leads to the increase of the total $J^{(2)}$-value at $\Omega_x \geq 0.45$ MeV. The shape of the peak

8

(plateau) in $J^{(2)}$ is determined by a delicate balance between alignments in the proton and neutron subsystems which depends on deformation, rotational frequency and Fermi energy. For example, no increase in the total dynamic moment of inertia $J^{(2)}$ has been found in the calculations after the peak up to $\Omega_x = 0.5$ MeV in ^{192}Hg, see Fig. 4. It is also of interest to mention that the sharp increase in $J^{(2)}$ of the yrast SD band in ^{190}Hg is also reproduced in the present calculations. One should note that the CRHB calculations slightly overestimate the magnitude of $J^{(2)}$ at the highest observed frequencies. The possible reasons could be the deficiencies either of the Lipkin-Nogami method [46] or the cranking model in the band crossing region or both of them.

5   Conclusions

The applications of the cranked versions of the relativistic mean field theory to the description of superdeformed bands in different mass regions clearly indicates that this theory provides very good agreement with experimental data. The level of agreement is comparable and in many cases better than the one obtained in the non-relativistic approaches.

References

[1] Bengtsson, R. *et al.*, Phys. Lett. **57B**, 301 (1975).

[2] Neergård, K. and Pashkevich, V. V., Phys. Lett. **59B**, 218 (1975).

[3] Twin, P. J. *et al.*, Phys. Rev. Lett. **57**, 811 (1986).

[4] Svensson, C. E. *et al.*, Phys. Rev. Lett. **82**, 3400 (1999).

[5] Devlin, M. *et al.*, Phys. Rev. Lett. **82**, 5217 (1996).

[6] Singh, B., Firestone, R. B. and Chu, S. Y. F., Nuclear Data Sheets **78**, 1 (1996).

[7] Afanasjev, A. V., Lalazissis, G. A. and Ring, P., Nucl. Phys. **A634**, 395 (1998).

[8] Bengtsson, T., Ragnarsson, I. and Åberg, S., Phys. Lett. **B208**, 39 (1988).

[9] Nazarewicz, W., Wyss R. and Johnson, A., Nucl. Phys. **A503**, 285 (1989).

[10] Shimizu, Y. R., Vigezzi, E. and Broglia, R. A., Nucl. Phys. **A509**, 80 (1990).

[11] Satuła, W., Ćwiok, S., Nazarewicz, W., Wyss, R. and Johnson, A., Nucl. Phys. **A529**, 289 (1991).

[12] Bonche, P., Flocard, H, and Heenen, P. H., Nucl. Phys. **A467**, 115 (1987).

[13] Girod, M., Delaroche, J. P., Berger, J. F. and Libert, J., Phys. Lett. **B325**, 1 (1994).

[14] Egido, J. L. and Robledo, L. M., Phys. Rev. Lett. **70**, 2876 (1993).

[15] Koepf, W. and Ring, P., Nucl. Phys. **A493**, 61 (1989).

[16] Koepf, W., and Ring, P., Nucl. Phys. **A511**, 279 (1990).

[17] Afanasjev, A. V., König, J. and Ring, P., report nucl-th/9907105 and to be published.

[18] Åberg, S., Flocard, H. and Nazarewicz, W., Ann. Rev. Nucl. Part. Sci. **40**, 439 (1990).

[19] Baktash, C., Haas, B. and Nazarewicz, W., Ann. Rev. Nucl. Part. Sci. **45**, 485 (1995).

[20] Dobaczewski, J., Proc. of conf. "Nuclear structure 98", Gatlinburg, Tennessee, USA, 1998, (Edited by C. Baktash), AIP 481, in press, (see also nucl-th/9811043)

[21] Serot, B. D. and Walecka, J. D., Adv. Nucl. Phys. **16**, 1 (1986).

[22] König, J. and Ring, P., Phys. Rev. Lett. **71**, 3079 (1993).

[23] Kaneko, K., Nakano, M. and Matsuzaki, M., Phys. Lett. **B317**, 261 (1993).

[24] Madokoro, H. and Matsuzaki, M., Phys. Rev. **C56**, R2934 (1997).

[25] Reinhard, P.-G., Rufa, M., Maruhn, J., Greiner, W. and Friedrich, J., Z. Phys. **A323**, 13 (1986).

[26] Kurcharek, H. and Ring, P., Z. Phys. **A339**, 23 (1991).

[27] Lalazissis, G. A., Vretenar, D. and Ring, P., Phys. Rev. **C57**, 2294 (1998).

[28] Pöschl, W., Vretenar, D., Lalazissis, G. A. and Ring, P., Phys. Rev. Lett. **79**, 3841 (1997).

[29] Vretenar, D., Lalazissis, G. A. and Ring, P., Phys. Rev. Lett. **82**, 4595 (1999).

[30] Lipkin, H. J., Ann. Phys. **31**, 525 (1960).

[31] Nogami, Y., Phys. Rev. **134**, 313 (1964).

[32] Pradhan, H. C., Nogami, Y., and Law, J., Nucl. Phys. **A201**, 357 (1973).

[33] Afanasjev, A. V., König, J. and Ring, P., Nucl. Phys. **A608**, 107 (1996).

[34] Quentin, P. and Flocard, H., Ann. Rev. Nuc. Part. Sci. **28**, 523 (1978).

[35] Dobaczewski, J. and Dudek, J., Phys. Rev. **C52**, 1827 (1995).

[36] Ring, P., Prog. Part. Nucl. Phys. **37**, 193 (1996).

[37] Ring, P. and Schuck, P., "The Nuclear Many-body Problem" (Springer Verlag, Heidelberg, 1980)

[38] Bengtsson, T. and Ragnarsson, I., Nucl. Phys. **A436**, 14 (1985)..

[39] Nazarewicz, W., Dudek, J., Bengtsson, R., Bengtsson, T. and Ragnarsson, I., Nucl. Phys. **A435**, 397 (1985).

[40] Dudek, J., Nazarewicz, W., and Olanders, P., Nucl. Phys. **A420**, 285 (1984).

[41] Karlsson, L. B., Ragnarsson, I. and Åberg, S., Nucl. Phys. **A639**, 654 (1998).

[42] Afanasjev, A. V., Fossan, D. B., Lane, G. J. and Ragnarsson, I., Physics Reports, in press

[43] Satuła, W., Wyss, R., and Magierski, P., Nucl. Phys. **A578**, 45 (1994).

[44] Zheng, D. C., Sprung D. W. L. and Flocard, H., Phys. Rev. **C46**, 1355 (1992).

[45] Dobaczewski, J. and Nazarewicz, W., Phys. Rev. **C47**, 2418 (1993).

[46] Magierski, P., Ćwiok, S., Dobaczewski, J., and Nazarewicz, W., Phys. Rev. C **48**, 1686 (1993).

[47] Ragnarsson, I., Phys. Lett. **B264**, 5 (1991).

[48] Ragnarsson, I., Nucl. Phys. **A557**, 167c (1993).

[49] L. B. Karlsson. PhD Thesis, Lund Institute of Technology, Lund 1999, and to be published

[50] Shimizu, Y. R., Garrett, J. D., Broglia, R. A., Gallardo, M. and Vigezzi, E., Rev. Mod. Phys. **61**, 131 (1989).

[51] Afanasjev, A. V. Lalazissis, G. A., and Ring, P., Acta Phys. Hung. N. S., Heavy Ion Physics **6**, 299 (1997).

[52] Ring, P., Afanasjev, A. V. and Meng, J., "Contemporary Nuclear Shell Models". (Edited by X.-W. Pan, D. H. Feng, M. Vallieres) (Springer-Verlag, Berlin, Heidelberg, New York, 1997) p. 274.

[53] Ring, P. and Afanasjev, A. V., Prog. Part. Nucl. Phys., **38**, 137 (1997).

[54] Afanasjev, A. V. and Ring, P., Nucl. Phys. A, in press, report nucl-th/9907104

[55] Satuła, W., Dobaczewski, J., Dudek, J. and Nazarewicz, W., Phys. Rev. Lett. **77**, 5182 (1996).

[56] Bonche, P., Flocard, H., and Heenen, P.-H., Nucl. Phys. **A598**, 169 (1996).

[57] El Aouad, N. *et al*, report nucl-th/9612048

[58] Rigollet, C., Bonche, P., Flocard, H. and Heenen, P.-H., Phys. Rev. **C59**, 3120 (1999).

[59] Afanasjev, A. V., Ragnarsson, I. and Ring, P., Phys. Rev. **C59**, 3166 (1999).

[60] Ragnarsson, I., Janzen, V. P., Fossan, D. B., Schmeing, N. C. and Wadsworth, R., Phys. Rev. Lett. **74**, 3935 (1995).

[61] Afanasjev, A. V. and Ragnarsson, I., Nucl. Phys. **A591**, 387 (1995).

[62] Ragnarsson, I., Phys. Lett. **B199**, 317 (1987).

[63] Rudolph, D. *et al.*, Phys. Rev. Lett. **80**, 3018 (1998).

[64] Rudolph, D. *et al.*, Phys. Rev. Lett. **82**, 3763 (1999).

[65] Rudolph, D. *et al*, Nucl. Phys. **A630**, 417c (1998).

[66] Madokoro, H. and Matsuzaki, M., Prog. Theor. Phys. **101**, 1027 (1999).

[67] Sun, Y., Zhang, J., Guidry, M. and Wu, C.-L., Phys. Rev. Lett., **83**, 686 (1999).

[68] Girod, M., Delaroche, J. P., Berger, J. F., Peru, S. and Libert, J., Z. Phys. **A358**, 177 (1997).

[69] Valor, A., Egido, J. L. and Robledo, L. M., Phys. Lett. **B392**, 249 (1997).

[70] Villafranca, A. and Egido, J. L., Phys. Lett. **B408**, 35 (1997).

[71] Libert, J., Berger, J. F., Delaroche, J. P. and Girod, M., Nuc. Phys. **A553**, 523c (1993).

[72] Gall, B., Bonche, P., Dobaczewski, J., Flocard, H. and Heenen, P.-H, Z. Phys. **A348**, 183 (1994).

[73] Heenen, P.-H., Bonche, P., and Flocard, H., Nucl. Phys. **A588**, 490 (1995).

[74] Terasaki, J., Heenen, P.-H., Bonche, P., Dobaczewski, J. and Flocard, H., Nucl. Phys. **A593**, 1 (1995).

[75] Terasaki, J., Flocard, H., Heenen, P.-H. and Bonche, P., Phys. Rev. **C55**, 1231 (1997).

[76] Heenen, P.-H. and Janssens, R. V. F., Phys. Rev. **C57**, 159 (1998).

[77] Satuła, W., and Wyss, R., Phys. Rev. **C50**, 2888 (1994).

[78] Wyss, R., and Satuła, W., Phys. Lett. **B351**, 393 (1995).

[79] Sun, Y., Zhang, J. and Guidry, M., Phys. Rev. Lett. **78**, 2321 (1997).

[80] Berger, J. F., Girod, M. and Gogny, D., Comp. Phys. Comm. **63**, 365 (1991).

[81] Lalazissis, G. A. and Ring, P., Phys. Lett. **B427**, 225 (1998).

[82] McNabb, D. P. *et al.*, Phys. Rev. **C56**, 2474 (1997).

[83] Gall, B. J. P. *et al.*, Phys. Lett. **B345**, 124 (1995).

[84] Lopez-Martens, A. *et al.*, Phys. Lett. **B380**, 18 (1996).

[85] Hauschild, K. *et al.*, Phys. Rev. **C55**, 2819 (1997).

[86] van Severen, U. J. *et al.*, Z. Phys. **A353**, 15 (1995).

[87] Wilson, A. N. *et al.*, Phys. Rev. **C54**, 559 (1996).

[88] Fallon, P. *et al.*, Phys. Rev. **C51**, R1609 (1995).

[89] Cederwall, B. *et al.*, Phys. Rev. Lett. **72**, 3150 (1994).

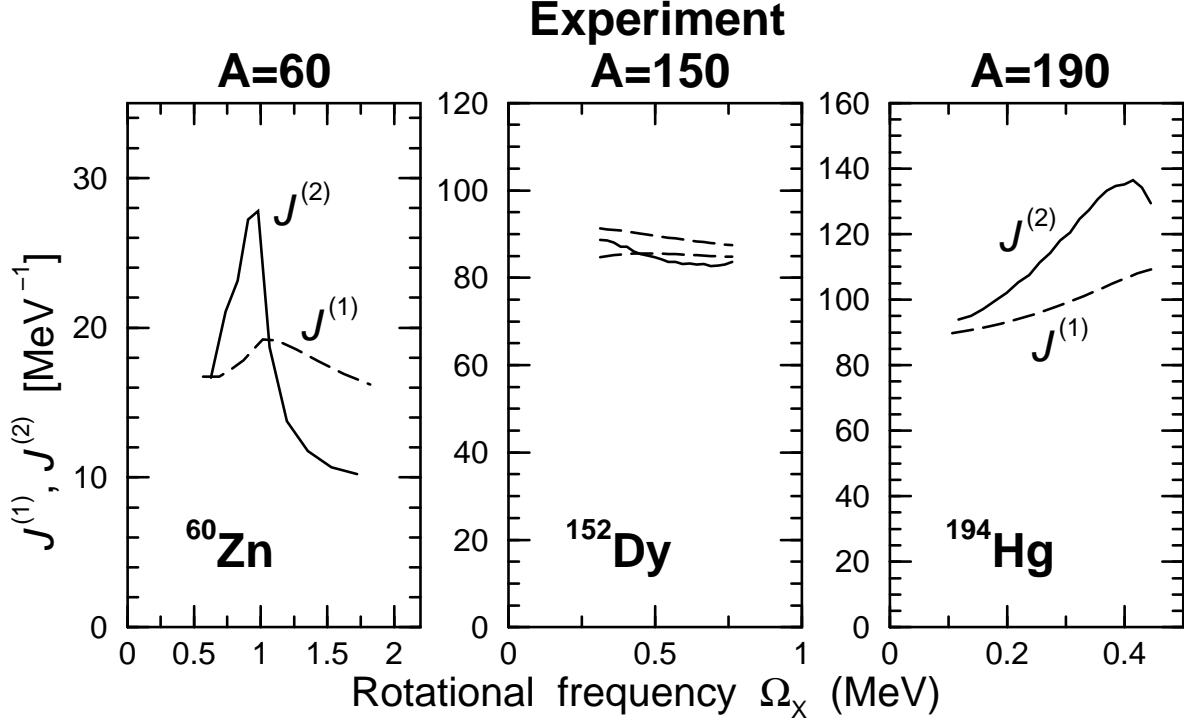[90] Khoo, T. L. *et al.*, Phys. Rev. Lett. **76**, 1583 (1996).

Figure 1: Dynamic ($J^{(2)}$) and kinematic ($J^{(1)}$) moments of inertia of representative SD bands observed in the $A \sim 60$, 150 and 190 mass regions. SD bands in ^{60}Zn and ^{194}Hg are linked to the low-spin level scheme. On the contrary, no SD band in $A \sim 140 - 150$ mass region is linked to the low-spin level scheme. Thus the $J^{(1)}$ values for the SD band in ^{152}Dy are shown under two different spin assignments: the lowest transition in SD band with energy 602.4 keV corresponds to the spin changes of $26^+ \rightarrow 24^+$ (lowest curve) and of $28^+ \rightarrow 26^+$ (highest curve). One should note that the analysis based both on the effective alignment approach and the systematics of experimental estimations of the spins of the lowest states in the SD bands in this mass region favours the first alternative, however, the second alternative cannot be excluded, see Ref. [7] for details.
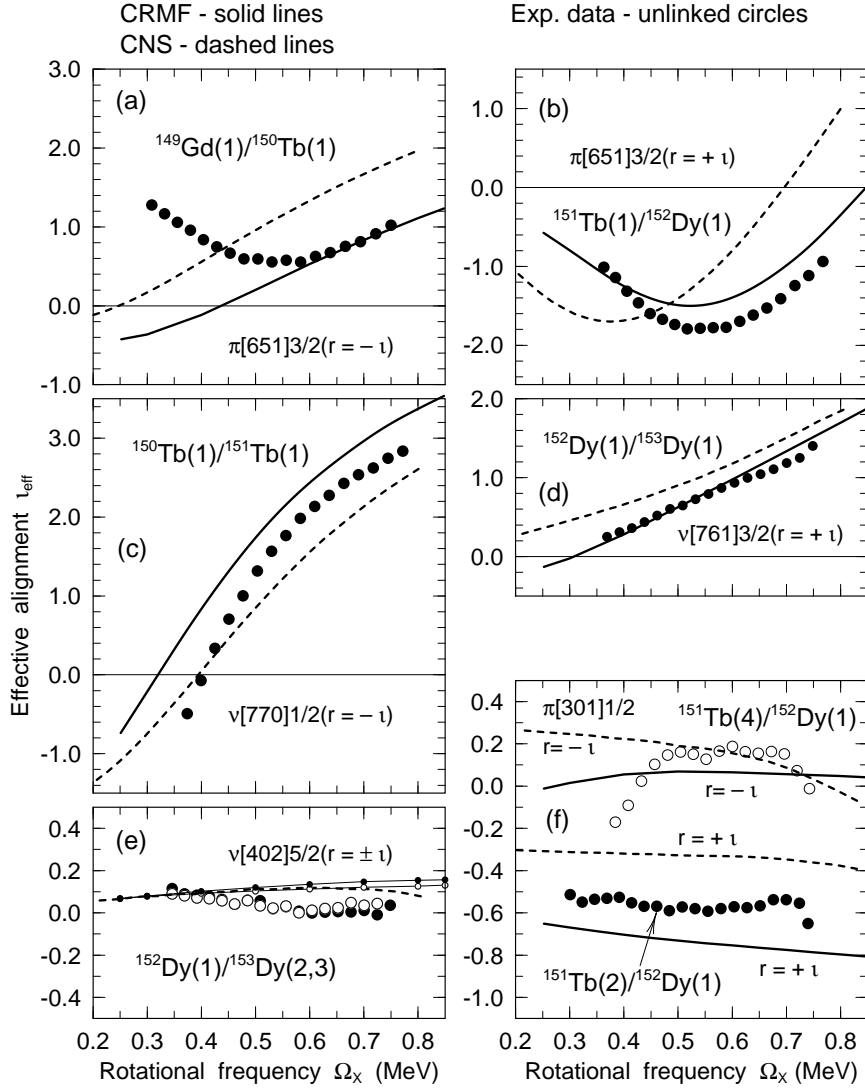
Figure 2: Effective alignments, i_{eff} (in units $\hbar$), extracted from experimental data are compared with those extracted from the corresponding configurations calculated in the CRMF theory and in the configuration-dependent cranked Nilsson-Strutinsky (CNS) approach based on the Nilsson potential. The experimental effective alignment between bands A and B is indicated as 'A/B'. The band A in the lighter nucleus is taken as a reference, so the effective alignment measures the effect of the additional particle. The compared calculated configurations differ in the occupation of the orbitals shown in the panels. (From results obtained in Refs. [7, 48]).
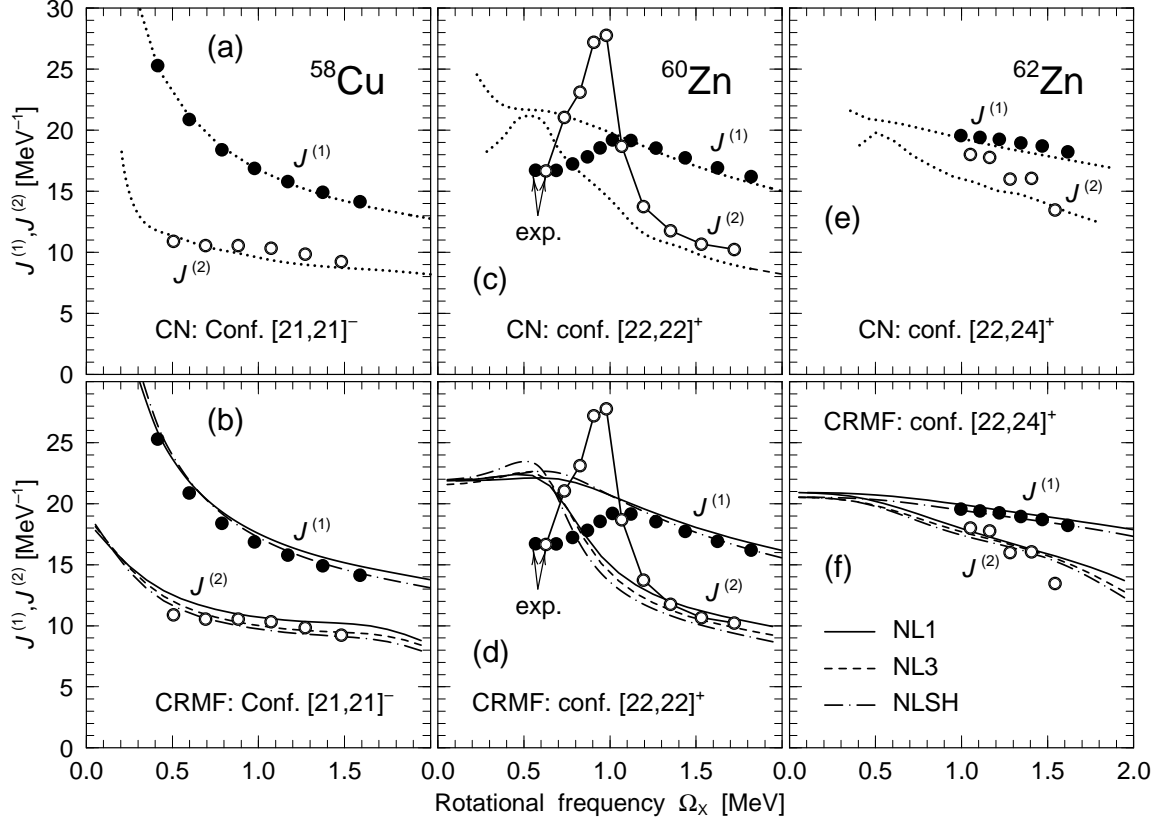
Figure 3: Kinematic $J^{(1)}$ (unlinked solid circles) and dynamic $J^{(2)}$ (open circles) moments of inertia of observed bands versus the ones of assigned calculated configurations. The notation of the lines is given in the figure. To label the configurations we use the shorthand notation $[p_1 p_2, n_1 n_2]$ where p_1 (n_1) is the number of proton (neutron) $f_{7/2}$ holes and p_2 (n_2) is the number of proton (neutron) $g_{9/2}$ particles. Superscripts to the configuration labels (e.g. $[22, 22]^+$) are used to indicate the sign of the signature r for that configuration ($r = \pm 1$). The values of $J^{(1)}$ calculated with NL3 are typically in between the ones obtained with NL1 and NLSH, so for simplicity they are not shown. (From Ref. [59]).
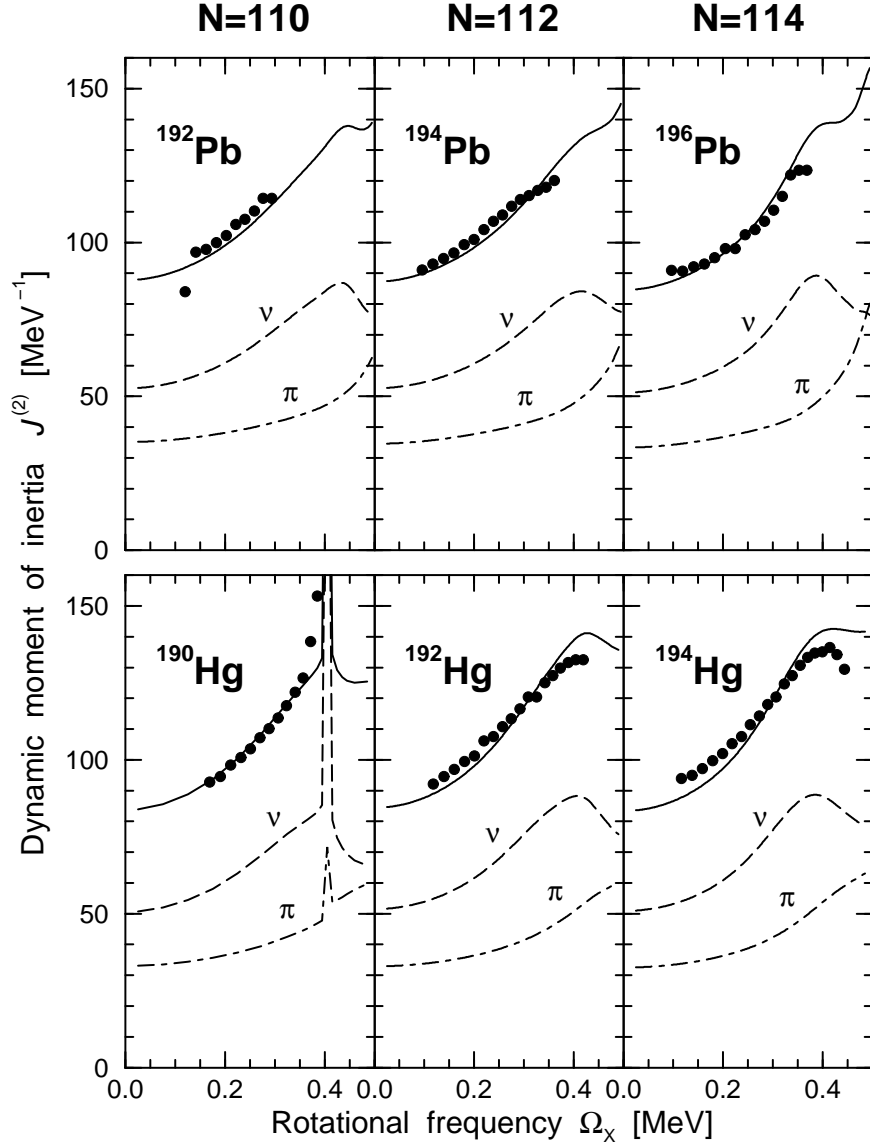
Figure 4: Dynamic moments of inertia $J^{(2)}$ of observed (solid circles) yrast SD bands in the ^{190,192,194}Hg and ^{192,194,196}Pb nuclei versus the ones of calculated lowest in energy SD configurations. Solid lines show the total calculated dynamic moments of inertia $J^{(2)}$, while long-dashed and dash-dotted lines show the contribution in $J^{(2)}$ from neutron and proton subsystems. The experimental data are taken from Refs. [82] (^{192}Pb), [83, 84, 85] (^{194}Pb), [86] (^{196}Pb), [87] (^{190}Hg), [88] (^{192}Hg) and [89, 90] (^{194}Hg).
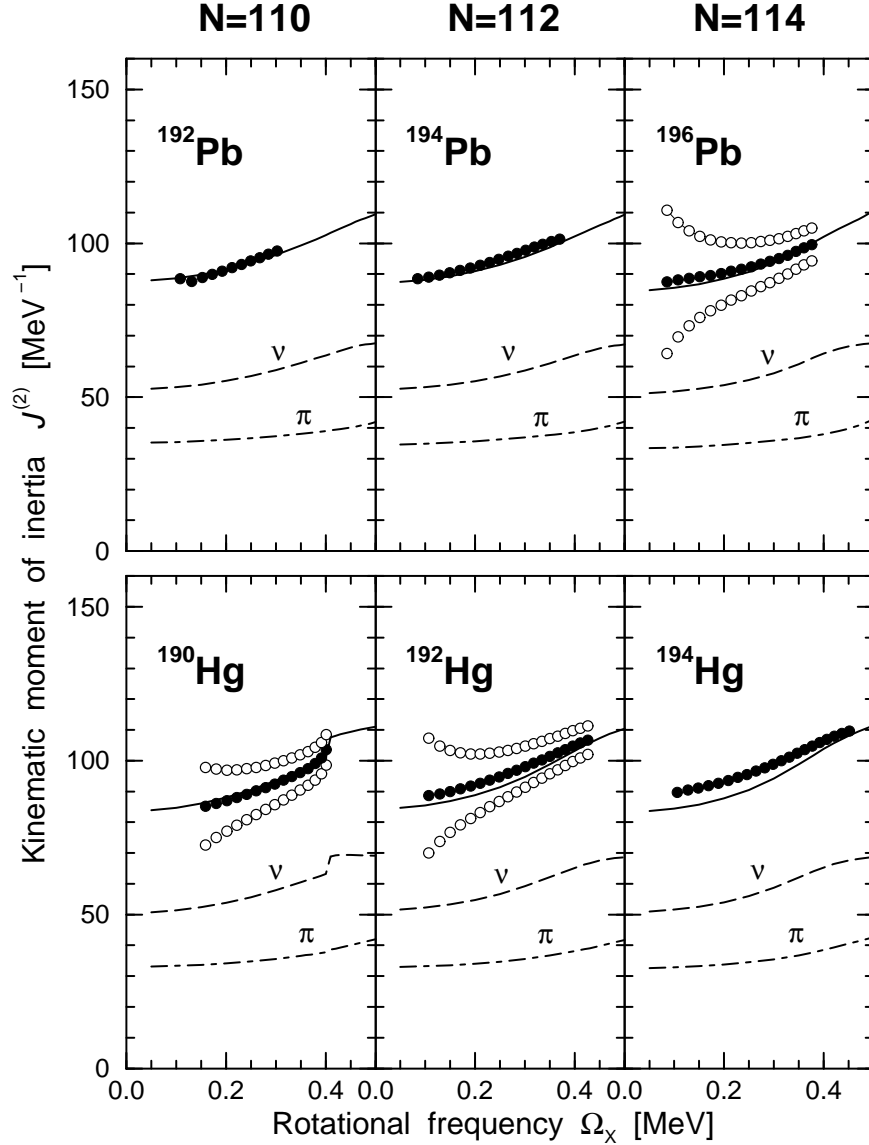
Figure 5: The same as Fig. 4 but for kinematic moments of inertia $J^{(1)}$. Only in the cases of the yrast SD bands in ^{192,194}Pb [82, 84, 85] and ^{194}Hg [90], the spins of the bands are firmly (^{194}Hg, ^{194}Pb) or tentatively (^{192}Pb) defined in experiment. In other cases, the 'experimental' kinematic moments of inertia $J^{(1)}$ are shown for three different spin values of the lowest state I_0 in SD band, which are consistent with the signature of the lowest calculated SD configuration. The $J^{(1)}$ values obtained in such a way are shown by circles with values being in best agreement with calculations indicated by solid circles. These comparisons indicate that the lowest transitions in the yrast SD bands of ^{190}Hg, ^{192}Hg and ^{196}Pb with energies 316.9, 214.4 and 171.5 keV, respectively, most likely correspond to the spin changes of $14^+ \to 12^+$, $10^+ \to 8^+$ and $8^+ \to 6^+$.